Martin J. Schäfer, Stephan G. Jantz and Henning A. Höppe*

The UV-phosphor strontium fluorooxoborate $Sr[B_5O_7F_3]$:Eu

https://doi.org/10.1515/znb-2019-0174
Received October 31, 2019; accepted November 19, 2019

Abstract: The fluorooxoborates $Sr[B_5O_7F_3]$ ($Ccm2_1$ (no. 36), $Z=4$, $a=864.777(3)$ pm, $b=1001.037(4)$ pm, $c=810.110(5)$ pm, 630 refl., 68 param., $R_F=0.061$, $R_{Bragg}=0.051$) and $Sr[B_5O_7F_3]$:Eu^{2+} were synthesized via solid-state reactions from $Sr(BF_4)_2$ and B_2O_3. Doping was achieved by adding EuF_3, which was reduced to its divalent state during the synthesis. $Sr[B_5O_7F_3]$ was investigated by infrared spectroscopy. Photoluminescence spectra of the doped compound revealed an Eu^{2+} 5*d*-4*f* emission in the UV regime peaking at 371 nm with a full width at half maximum (FWHM) of 21 nm upon excitation at 239 nm, which proves a weak coordination of europium by the anionic fluorooxoborate network.

Keywords: europium; fluorooxoborates; infrared spectroscopy; luminescence spectroscopy; strontium.

Dedicated to: Professor Arndt Simon on the occasion of his 80th birthday.

1 Introduction

In the course of our systematic investigations of the broad field of silicate-analogous materials [1–3] we also came across compounds comprising BO_3F tetrahedra, i.e. fluorooxoborates; systems generated through the formal addition of fluoride anions to boron compounds comprising BO_3 triangles are of interest in applications as host materials for luminescence or as NLO materials [4–6]. Surprisingly, one of these, $Sn[B_2O_3F_2]$, represents as precursor for borates not accessible otherwise, like the first crystalline tin borate $Sn_3[B_4O_9]$ [2]. Such host structures should provide significantly weaker coordination strength, i.e. smaller ligand fields than the respective oxides. Accordingly, we substituted Eu^{2+} into our new and apparently very weakly coordinating barium fluorooxoborate $Ba[B_4O_6F_2]$ [6], in which europium is situated on the barium sites. Divalent europium normally causes broad-band emissions due to parity allowed 5*d*-4*f* emissions; contrarily to the 4*f*, the 5*d* states are subject to nephelauxetic and ligand field effects, and thus the recorded emission strongly depends on the nature of the ligand atoms. Therefore emissions from the deep red to the deep UV can be caused by strongly and weakly coordinating host structures, respectively. In case of the aforementioned $Ba[B_4O_6F_2]$:Eu we observed a rarely seen narrow-banded 4*f*-4*f* emission ($^6P\rightarrow{}^8S$) at 359 nm at room temperature on top of the commonly known broad 5*d*-4*f* band peaking around 366 nm; such transitions had previously only been observed for pure fluorides. Such emissions in the deep UV are of interest for water disinfection purposes. Fluorooxoborates are less reactive than metal fluorides against glass and other materials. The sensibility of divalent europium towards nephelauxetic and ligand field changes can be tuned by just replacing the alkaline earth host by a larger or smaller element allowing for less or more direct influence of the ligand atoms on the 5*d* states.

For the work described in this contribution we chose divalent strontium, which is often used in host materials for Eu^{2+} due to the same size and charge, both being beneficial for efficient doping. Our efforts yielded $Sr[B_5O_7F_3]$, the crystal structure of which had been published [7, 8] just before our own synthesis was successful. Here we present our own synthetic approach to this fluorooxoborate. Its crystal structure was re-investigated by means of powder X-ray diffraction and its luminescence properties after doping with Eu^{2+} were investigated.

2 Results and discussion

2.1 Crystal structure

$Sr[B_5O_7F_3]$ crystallises in the same structure type as its calcium counterpart, which was published as $Ca_2[B_{10}O_{14}F_6]$ with a doubled sum formula but half the formula units per unit cell. The title compound adopts the non-centrosymmetric space group $Ccm2_1$. The fundamental building block (FBB) is shown in Fig. 1 and consists of two trigonal

***Corresponding author: Henning A. Höppe,** Lehrstuhl für Festkörperchemie, Institut für Physik, Universität Augsburg, Universitätsstraße 1, 86159 Augsburg, Germany, Fax: 0821-598-5955, E-mail: henning@ak-hoeppe.de
Martin J. Schäfer and Stephan G. Jantz: Lehrstuhl für Festkörperchemie, Institut für Physik, Universität Augsburg, Universitätsstraße 1, 86159 Augsburg, Germany

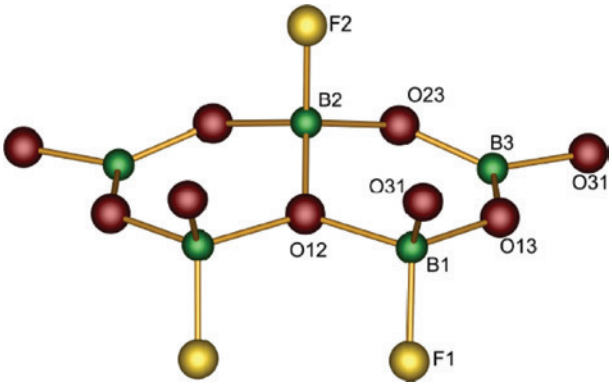

Fig. 1: FBB of $Sr[B_5O_7F_3]$, featuring the slightly bent bicyclic structure. Boron atoms in green, oxygen atoms in red, fluorine atoms in yellow.

planar BO_3 units and three BO_3F tetrahedra; two tetrahedra and one BO_3 triangle form a six-membered ring. Two of those rings are condensed via a common edge and thus the FBB can be described according to Burns et al. [9] by the descriptor $2\Delta3\square:[\Phi]<\Delta2\square>|<\Delta2\square>|$.

The FBBs are connected via common O31[2] oxygen atoms bridging two adjacent boron atoms to form layers in the (100) plane. Thus, four FBBs form an 18-membered ring, in which the strontium atoms are situated. All fluorine atoms point out of the planes (Fig. 2). The atoms O12, B2 and F2 lie on a mirror plane together with the shared edge. Table 1 summarizes selected interatomic distances and angles.

An unusual feature of the structure is the oxygen atom O12[3] connecting three adjacent BO_3F tetrahedra within the FBB. The distances between O12[3] and the neighbouring boron atoms B1 and B2 are 157.4(17) and 142.6(17) pm, respectively, and thus considerably larger than usual $B_\square$–O[2] bonds (see caption to Table 1 for definition of $B_\square$ and B_Δ) which are usually in the range from 145 to 147 pm, as observed in $Sn[B_2O_3F_2]$ and $Ba[B_4O_6F_2]$ [5, 6]. Such rarely found three-fold-coordinated oxygen atoms O[3] were reported before in borates like $Ni_3B_{18}O_{28}(OH)_4 \cdot H_2O$ or $LiBa_3(OH)[B_9O_{16}][B(OH)_4]$ [10, 11], and in alumosilicates like $Be_3Al_2Si_6O_{18}$ or $SiAl_2O_5$ [12–14]. The average B–O bond lengths in the title compound of 137 pm (B_Δ–O) and 148 pm ($B_\square$–O) agree well with the sum of the ionic radii [15]. Yet the variance of the bond lengths is slightly larger, compared with other, similar compounds. This variance, as well as the elongated bonds with the O12 atom are also reflected in the slightly larger but still uncritical deviations of the tetrahedral units from a regular tetrahedron, calculated according to Balic-Žunic and Makovicky [16, 17] to be 0.68% (B1) and 0.27% (B2).

The strontium cation is situated within the layers of the anionic substructure, in a ring built up by four

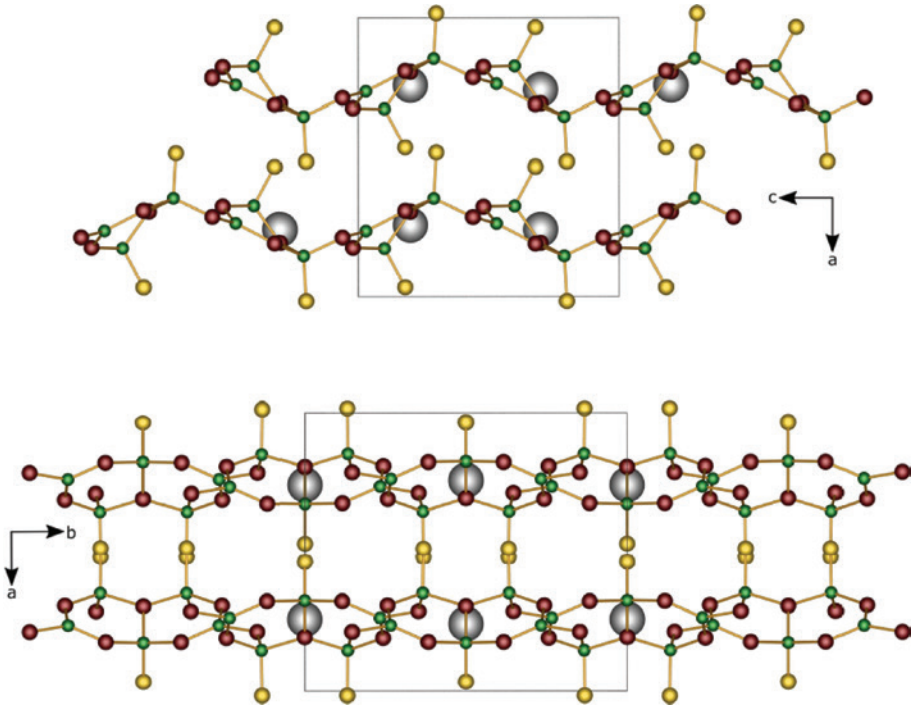

Fig. 2: Layers of $Sr[B_5O_7F_3]$ viewed along the [010] direction (upper picture) and the [001] direction (lower picture). Strontium atoms in grey, boron atoms in green, oxygen atoms in red, fluorine atoms in yellow.

Table 1: Selected interatomic distances and angles in $Sr[B_5O_7F_3]$; standard deviations in parentheses; $B_{\triangle}$ represents trigonal planar coordinated and $B_{\square}$ represents tetrahedrally coordinated boron atoms.

Atoms	Coordination number	Distance/pm	Ø/pm
Sr–O	6(O) + 3(F)	258.4(6)–261.6(4)	259(2)
Sr–F		239.4(5)–261.6(4)	252(9)
$B_{\triangle}$–O	3	134.6(12)–141.5(11)	137(3)
$B_{\square}$–O	3(O) + 1(F)	138.4(11)–157.4(12)	148(6)
$B_{\square}$–F		139.1(15)–141.5(10)	140(1)
O12–B1	3	142.6(17)	
O12–B2		157.4(12)	
		Angle/deg	**Ø/deg**
O–$B_{\triangle}$–O		116.4(9)–122.0(9)	119.8(3)
O–$B_{\square}$–O		102.0(8)–112.6(1.1)	109.6(4)
O–$B_{\square}$–F		105.3(8)–113.5(1.1)	109.2(3)
B–O12–B		116.8(11)–118.7(13)	118.1(9)

$B_5O_7F_3^{2-}$ FBBs. Its nine-fold coordination consists of six oxygen atoms of the aforementioned ring and by three fluorine atoms of the layers above and below. The coordination polyhedron can be described as a strongly distorted triangular cupola (Johnson solid J_3). The Sr–O distances range from 258 to 262 pm, which is slightly shorter than the sum of their ionic radii (267 pm) [15]. The Sr–F distances are quite different, as the different fluorine anions F1 and F2 coordinate the strontium cation from different layers. Both distances (239 pm for Sr–F1, 256 pm for Sr–F2) are shorter than the sum of their ionic radii (260 pm).

2.2 Infrared Spectroscopy

The IR spectrum of $Sr[B_5O_7F_3]$ was recorded in the range from 4000 to 400 cm^{-1} (Fig. 3). The inset shows the whole measured area with only very weak bands caused by traces of adhesive moisture beyond 3000 cm^{-1}. The assignments listed in Table 2 are based on the infrared spectrum of $Ba[B_4O_6F_2]$ and confirmed by DFT calculations, as well as on other reference data [18, 19]. As expected, considering the comparable structural units (BO_3 and BO_3F), the spectra are similar. The bands around 1500–1275 cm^{-1} and the band near 960 cm^{-1} are caused by the asymmetric and symmetric stretching modes of the trigonal BO_3 units. According to our calculations on comparable infrared spectra [5, 6] the asymmetric and symmetric stretching modes of the B–O bonds of tetrahedral BO_3F units are found in the regimes 1100–980 and 960–850 cm^{-1}, respectively. Characteristic stretching modes of B–F bonds in

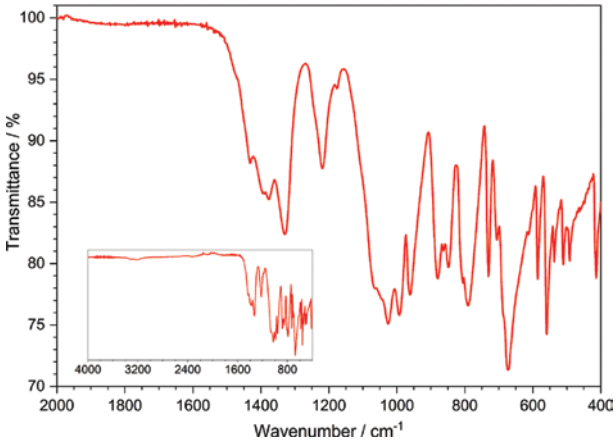

Fig. 3: IR spectrum of $Sr[B_5O_7F_3]$; the inset shows the complete region up to 4000 cm^{-1}.

Table 2: IR bands of $Sr[B_5O_7F_3]$, as well as their assignments, using data from $Ba[B_4O_6F_2]$ [6].

IR/cm^{-1}	Assignment
1500–1275	$\nu_{as}(BO_3)$
1220	$\nu(OB_3)$
1063	ν_{as}(B–O) in BO_3F
1027	ν_{as}(B–O) in BO_3F
992	ν(B–F) in BO_3F
960	$\nu_s(BO_3)$
880	$\delta(BO_3F)$, ν_s(B–O), ν(B–F) in BO_3F (?)
848	ν_s(B–O), ν(B–F) in BO_3F

fluorooxoborates are found in the regimes 1000–920 and 860–730 cm^{-1}, deformation modes of BO_3F tetrahedra typically lie around 860 cm^{-1} for the similar $Ba[B_4O_6F_2]$ [6]. Based on these regimes we tentatively assigned the experimentally observed modes of the title compound according to Table 2. Aside from a slight shift in wavenumbers for most bands, the most obvious difference is an additional band around 1220 cm^{-1} in the spectrum of $Sr[B_5O_7F_3]$. This was also reported by Mutailipu et al. [7], but was not explained further. We suspect that this band is caused by B–O stretching vibrations including the three-fold-coordinated $O12^{[3]}$ as it does not appear in $Ba[B_4O_6F_2]$. A $B–O^{[3]}$ bond is presumably weaker than a $B–O^{[2]}$ bond causing a shift to smaller wavenumbers from the standard regime. The presence of an infrared band in this range in other borates featuring three-fold-coordinated oxygen [10, 20–22] supports our tentative assignment. A respective asymmetric mode is to be expected at lower frequencies, maybe the sharp vibration around 720 cm^{-1} might fit – but this is rather speculative as the spectrum is very busy in this regime.

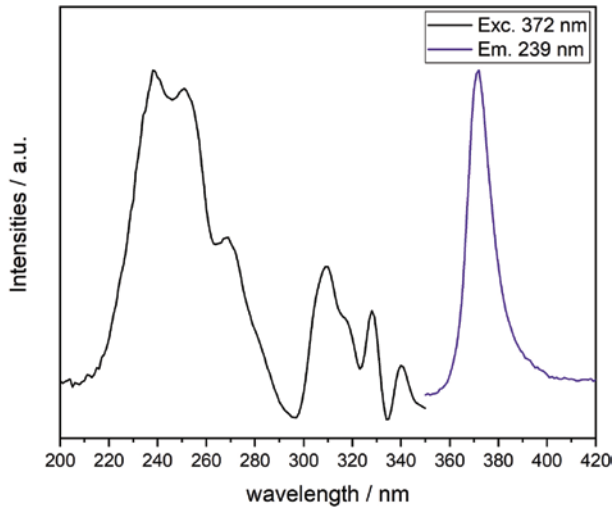

Fig. 4: Photoluminescence spectrum of $Sr[B_5O_7F_3]:Eu^{2+}$; emission spectrum (violet line) measured at $\lambda_{exc} = 239$ nm, excitation spectrum (black line) measured at $\lambda_{em} = 372$ nm.

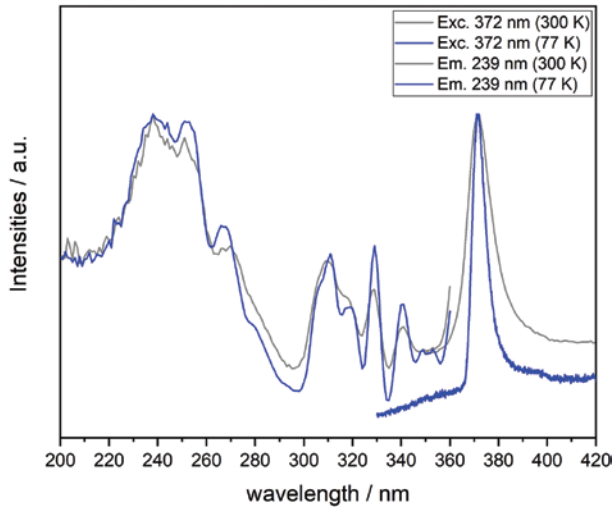

Fig. 5: Photoluminescence spectrum of $Sr[B_5O_7F_3]:Eu^{2+}$; emission and excitation at liquid nitrogen temperature (blue line) and room temperature (grey line); the spectra were measured with $\lambda_{exc} = 239$ nm and $\lambda_{em} = 372$ nm, respectively.

2.3 Fluorescence spectroscopy on $Sr[B_5O_7F_3]:Eu^{2+}$

The fluorescence spectrum of $Sr[B_5O_7F_3]:Eu^{2+}$ (Fig. 4) features an emission with a single 5*d*-4*f* transition peaking at 372 nm with a full width at half maximum (FWHM) of 21 nm. The excitation spectrum comprises numerous peaks assigned to 4*f*-5*d* transitions. Below 370 nm, 4*f*-4*f* transitions of Eu^{2+} can be excited as well [23, 24], but they are hard to identify since the resolution of the spectrum is limited by the employed deuterium lamp. The width of all excitation peaks remains equal, even at lower temperatures, as shown in Fig. 5.

Compared to the fluorescence spectrum of $Ba[B_4O_6F_2]:Eu^{2+}$, the emission spectrum of $Sr[B_5O_7F_3]:Eu^{2+}$ shows no sharp peak which could be attributed to a 4*f*-4*f* transition, but the emission peak of the 5*d*-4*f* transition shows the same FWHM; this is reasonable as both host structures are quite similar. Both structures comprise layered polymeric fluorooxoborate anions; the cations situated in the voids of these layers are weakly coordinated by oxygen and fluorine atoms with large interatomic distances due to rather large coordination numbers ($Sr[B_5O_7F_3]$: 9, $Ba[B_4O_6F_2]$: 13). Since these distances are significantly shorter in the title compound compared to $Ba[B_4O_6F_2]$, it is not surprising that the emission wavelength is slightly red-shifted from 366 to 372 nm and that the 4*f*-4*f* transition cannot be observed in $Sr[B_5O_7F_3]:Eu^{2+}$ due to efficient relaxation from the ^6P (4*f*) to the 5*d* states. Nevertheless, the ligand field splitting and nephelauxetic effect of the 5*d* states in Eu^{2+} is still small enough that the emission of the *d*-*f* transition lies in the UV regime of the electromagnetic spectrum.

3 Conclusion

The effects observed for $Sr[B_5O_7F_3]:Eu^{2+}$ fit into the range of luminescence emissions which can be realised by Eu^{2+}-doped borates. With decreasing influence of the ligands introduced in the borate framework, borates are able to generate red (e.g. $Ba_2Mg(BO_3)_2:Eu^{2+}$), green (e.g. $Sr_3(BO_3)_2:Eu^{2+}$), blue (e.g. $BaNaB_9O_{15}:Eu^{2+}$), and violet (e.g. $SrB_4O_7:Eu^{2+}$) [25] emissions. Perovskite-like alkaline earth fluorides [26] or weakly coordinating silicates and sulphates [27, 28] and more recently the condensed fluorooxoborates $Sr[B_5O_7F_3]:Eu^{2+}$ and $Ba[B_4O_6F_2]:Eu^{2+}$ [6] have extended that trend into the deep UV regime, up to the point where 4*f*-4*f* emissions are observed as well in few cases. Investigations on further known alkaline earth fluorooxoborates like $Ca[B_5O_7F_3]$ [29], $Ba[BOF_3]$ [30] $Ba[B_5O_8F]\cdot H_2O$ [31] and $Ba[B_2O_3F_2]$ [32] doped with Eu^{2+} are under way and will be presented in due course.

4 Experimental Section

4.1 Synthesis of $Sr(BF_4)_2$

The synthesis of the starting material $Sr(BF_4)_2$ was achieved according to the following equation:

$$SrCO_3 + 2\,HBF_4 \rightarrow Sr(BF_4)_2 + H_2O + CO_2\uparrow$$

Three grams of $SrCO_3$ (20 mmol, Riedel-de Häen, 96% purity) were suspensed in 5 mL of demineralised water inside of a PVC container. 4.8 mL of HBF_4 (38 mmol, Alfa Aesar, 50% solution). The excess of $SrCO_3$ ensured the complete reaction of the tetrafluoroboric acid. The suspension was then filtered and the filtrate was slowly dried *in vacuo*, yielding phase-pure $Sr(BF_4)_2$.

4.2 Synthesis of $Sr[B_5O_7F_3]$ and $Sr[B_5O_7F_3]:Eu^{2+}$

The synthesis of $Sr[B_5O_7F_3]$ was achieved according to the following equation:

$$3\,Sr(BF_4)_2 + 9\,B_2O_3 \rightarrow 3\,Sr[B_5O_7F_3] + 2\,B_2O_3 + 5\,BF_3\uparrow$$

The pre-dried educts $Sr(BF_4)_2$ (255.0 mg, 0.9761 mmol) and B_2O_3 (160.0 mg, 2.298 mmol, Alfa Aesar, 99.999% purity) were weighed and ground in an agate mortar in air and transferred into a BN crucible. This mixture was dried at $T = 105$°C overnight in a compartment drier to get rid of any remaining moisture. The powder was then compressed inside the crucible which was then screwed and sealed in a silica ampoule under argon atmosphere. The sample was heated to 500°C with a rate of 50 K h^{-1}, held at that temperature for 500 h and then cooled to room temperature with a rate of 5 K h^{-1}. 263.1 mg (based on $Sr[B_5O_7F_3]$: 0.8469 mmol, 86.8% yield) of a slightly greyish, air and moisture insensitive powder were isolated.

For the synthesis of the doped sample, 1 mol% of the $Sr(BF_4)_2$ was replaced by EuF_3 (ChemPur, 99.9% purity). The mixture of dry educts was ground and pressed into a pellet inside of a glovebox and then filled into a silver crucible and sealed in a silica glass ampule under vacuum (2.5×10^{-3} mbar). The sample was heated to 500°C with a rate of 50 K h^{-1}, held at that temperature for 50 h and then cooled to 400°C in a first step and then to room temperature with the rates of 1 K h^{-1} and 40 K h^{-1}, respectively. The product was used for fluorescence spectroscopy without any further purification.

4.3 Spectroscopic methods

IR spectra were recorded on a Bruker EQUINOX 55 FT-IR spectrometer equipped with a Platinum ATR unit in the range 4000–400 cm^{-1} with a resolution of 4 cm^{-1} and 32 scans. Fluorescence excitation and emission spectra were recorded on a Horiba Fluoromax-4 spectrometer, scanning a range from 200 to 800 nm.

4.4 X-ray structure determination

The structure of $Sr[B_5O_7F_3]$ was solved from powder X-ray diffraction data. These data were collected on a Bruker D8 Advance capillary diffractometer in the range of $5.000 \le 2\theta \le 119.966°$, with steps of 0.02° and an irradiation of 36 s per step. The structure was solved by Direct Methods using the program EXPO2014 [33], further refinement was conducted with the program package FULLPROF

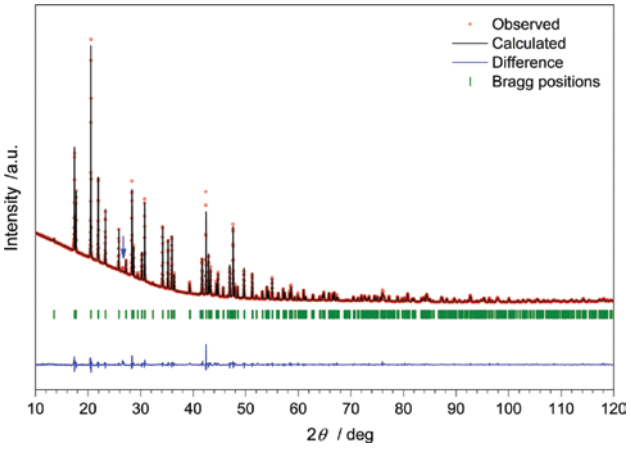

Fig. 6: Observed (red dots) and calculated (black line) powder diffraction pattern of $Sr[B_5O_7F_3]$, as well as the difference plot (blue line); the green vertical lines correspond to the possible Bragg-peak positions of $Sr[B_5O_7F_3]$; the only peak of a possible side phase (SrF_2) is labelled with a blue arrow.

Table 3: Parameters of the crystal structure determination of $Sr[B_5O_7F_3]$ (standard deviations in parentheses).

Sum formula	$Sr[B_5O_7F_3]$
Molar mass/g · mol^{-1}	310.67
Crystal system	Orthorhombic
Space group	$Ccm2_1$
a/pm	864.777(3)
b/pm	1001.037(4)
c/pm	810.110(5)
Volume/$\times 10^6$ pm^3	701.291(5)
Z	4
$\rho_{X\text{-ray}}$/g cm^{-3}	2.94
Diffractometer	Bruker D8 Advance
Radiation | λ/nm	Cu$K\alpha_{1,2}$ | 0.154056, 0.154439
Temperature/K	298(2)
2θ range/deg	5.000–119.966
Measured intensities	630
Refined parameters	68
R_P	0.020
R_{wP}	0.033
R_F	0.061
R_{Bragg}	0.051
χ^2	0.100

Table 4: Refined atomic coordinates, Wyckoff symbols and isotropic dislocation parameters U_{eq}/pm^2 in $Sr[B_5O_7F_3]$ (standard deviations in parentheses).

Atom	Wyckoff symbol	*x*	*y*	*z*	U_{eq}
Sr1	4*a*	0.25811(17)	0	0.29644[a]	88.7
B1	8*b*	0.8525(11)	0.8661(10)	0.2106(12)	126.7
B2	4*a*	0.6740(16)	0	0.4048(17)	126.7
B3	8*b*	0.7372(16)	0.7669(10)	0.4684(10)	126.7
O12	4*a*	0.8058(6)	0	0.2990(20)	126.7
O13	8*b*	0.8089(4)	0.7569(4)	0.3196(9)	126.7
O23	8*b*	0.6760(8)	0.8826(6)	0.5223(7)	126.7
O31	8*b*	0.7130(7)	0.6460(6)	0.5551(7)	126.7
F1	8*b*	0.0160(4)	0.8678(4)	0.2037(5)	126.7
F2	4*a*	0.5341(6)	0	0.3200(9)	126.7

[a]Fixed parameter.

[34] with the graphical interface WinPLOTR [35]. During the structure refinement, all atom positions were refined without any restraints. After some refinement cycles, the *z* position of the strontium atom was fixed to fix the structure along [001]. The XRD pattern including the refinement is portrayed in Fig. 6, the results of the structure refinement are listed in Tables 3 and 4.

Further details of the crystal structure investigation may be obtained from Fachinformationszentrum Karlsruhe, 76344 Eggenstein-Leopoldshafen, Germany (fax: +49-7247-808-555; e-mail: crysdata@fiz-karlsruhe.de, http://www.fiz-informationsdienste.de/en/DB/icsd/depot_anforderung.html) on quoting the deposition number CSD-1962709.

References

[1] P. Netzsch, P. Gross, H. Takahashi, S. Lotfi, J. Brgoch, H. A. Höppe, *Eur. J. Inorg. Chem.* **2019**, 3975.

[2] M. J. Schäfer, S. G. Jantz, H. A. Höppe, *Dalton Trans.* **2019**, *48*, 10398.

[3] P. Netzsch, P. Gross, H. Takahashi, H. A. Höppe, *Inorg. Chem.* **2018**, *57*, 8530.

[4] S. G. Jantz, L. van Wüllen, A. Fischer, E. Libowitzky, E. J. Baran, M. Weil, H. A. Höppe, *Eur. J. Inorg. Chem.* **2016**, 1121.

[5] S. G. Jantz, M. Dialer, L. Bayarjargal, B. Winkler, L. van Wüllen, F. Pielnhofer, J. Brgoch, R. Weihrich, H. A. Höppe, *Adv. Opt. Mater.* **2018**, 1800497.

[6] S. G. Jantz, F. Pielnhofer, L. van Wüllen, R. Weihrich, M. J. Schäfer, H. A. Höppe, *Chem. Eur. J.* **2018**, *24*, 443.

[7] M. Mutailipu, M. Zhang, B. Zhang, L. Wang, Z. Yang, X. Zhou, S. Pan, *Angew. Chem. Int. Ed.* **2018**, *57*, 6095.

[8] M. Luo, F. Liang, Y. Song, D. Zhao, F. Xu, N. Ye, Z. Lin, *J. Am. Chem. Soc.* **2018**, *140*, 3884.

[9] P. C. Burns, J. D. Grice, F. C. Hawthorne, *Can. Mineral.* **1995**, *33*, 1131.

[10] M. K. Schmitt, O. Janka, R. Pöttgen, K. Wurst, H. Huppertz, *Eur. J. Inorg. Chem.* **2017**, 3508.

[11] Q. Wei, J.-J. Wang, C. He, J.-W. Cheng, G.-Y. Yang, *Chem. Eur. J.* **2016**, *22*, 10759.

[12] L. A. Blaginina, A. F. Zatsepin, I. A. Dmitriev, *Fiz. Khim. Stekla* **1987**, *19*, 398.

[13] C. W. Burnham, *Z. Kristallogr.* **1963**, *118*, 337.

[14] J. B. Burt, N. L. Ross, R. J. Angel, M. Koch, *Am. Mineral.* **2006**, *91*, 319.

[15] R. D. Shannon, *Acta Crystallogr.* **1976**, *A32*, 751.

[16] T. Balic-Žunic, E. Makovicky, *Acta Crystallogr.* **1996**, *B52*, 78.

[17] E. Makovicky, T. Balic-Žunic, *Acta Crystallogr.* **1998**, *B54*, 766.

[18] J. Weidlein, U. Müller, K. Dehnicke, *Schwingungsfrequenzen I, Hauptgruppenelemente*, 1st edition, Georg Thieme Verlag, Stuttgart, New York **1981**.

[19] K. Nakamoto, *Infrared and Raman Spectra of Inorganic and Coordination Compounds*, Part A, 6th edition, John Wiley and Sons Inc., Hoboken **2009**.

[20] G. Sohr, V. Falkowski, M. Schauperl, K. R. Liedl, H. Huppertz, *Eur. J. Inorg. Chem.* **2015**, 527.

[21] D. A. Köse, B. Zümreoglu-Karan, T. Hökelek, E. Sahin, *Z. Anorg. Allg. Chem.* **2009**, *635*, 563.

[22] G. Sohr, D. M. Többens, J. Schmedt auf der Günne, H. Huppertz, *Chem. Eur. J.* **2014**, *20*, 17059.

[23] P. Dorenbos, *J. Lumin.* **2003**, *104*, 239.

[24] P. Dorenbos, *J. Phys.: Condens. Matter* **2003**, *15*, 575.

[25] A. Diaz, D. A. Keszler, *Mater. Res. Bull.* **1996**, *31*, 2, 105.

[26] R. A. Hewes, M. V. Hoffman, *J. Lumin.* **1971**, 261.

[27] F. M. Ryna, W. Lehmann, D. W. Feldman, J. Murphy, *J. Electrochem. Soc.* **1974**, *121*, 11, 1475.

[28] J. M. P. J. Verstegen, J. L. Sommerdijk, *J. Lumin.* **1974**, *9*, 297.

[29] Z. Zhang, Y. Wang, B. Zhang, Z. Yang, S. Pan, *Inorg. Chem.* **2018**, *57*, *9*, 4820.

[30] D. Jaing, Y. Wang, H. Li, Z. Yang, S. Pan, *Dalton Trans*. **2018**, *47*, 5157.

[31] C. Huang, G. Han, H. Li, F. Zhang, Z. Yang, S. Pan, *Dalton Trans.* **2019**, *48*, 6714.

[32] C. Huang, F. Zhang, H. Li, Z. Yang, H. Yu, S. Pan, *Chem. Eur. J.* **2019**, *25*, 6693.

[33] A. Altomare, C. Cuocci, C. Giacovazzo, A. Moliterni, R. Rizzi, N. Corriero, A. Falcicchio, *J. Appl. Crystallogr.* **2013**, *46*, 1231.

[34] J. Rodríguez-Carvajal, *Phys. B* **1993**, *192*, 55.

[35] T. Roisnel, J. Rodríguez-Carvajal, WinPLOTR, A Windows Tool for Powder Diffraction Pattern Analysis; see: T. Roisnel, J. Rodríguez-Carvajal, *Mater. Sci. Forum* **2001**, *378–3*, 118.